Neuropsychologia 138 (2020) 107340

Contents lists available at ScienceDirect

Neuropsychologia

journal homepage: http://www.elsevier.com/locate/neuropsychologia

Object parsing in the left lateral occipitotemporal cortex: Whole shape, part shape, and graspability

Wei Wu [a,b], Xiaoying Wang [a,b,**], Tao Wei [a,b], Chenxi He [a,b], Yanchao Bi [a,b,*]

[a] State Key Laboratory of Cognitive Neuroscience and Learning & IDG/McGovern Institute for Brain Research, Beijing Normal University, Beijing, 100875, China
[b] Beijing Key Laboratory of Brain Imaging and Connectomics, Beijing Normal University, Beijing, 100875, China

ARTICLE INFO

Keywords:
Object representation
Lateral occipitotemporal cortex
Shape
Grasping
fMRI

ABSTRACT

Small and manipulable objects (tools) preferentially evoke a network of brain regions relative to other objects, including the lateral occipitotemporal cortex (LOTC), which is assumed to process tool shape information. Given the correlation between various object properties, the exact type of information being represented in the LOTC remains debated. In three fMRI experiments, we examined the effects of multiple levels of shape (whole vs. object parts) and motor-related (grasping; manipulation) information. Combining representational similarity analysis and commonality analysis allowed us to partition the unique and shared effects of correlated dimensions. We found that grasping manner (for pickup), not the overall object shape or manner of manipulation, uniquely explained the LOTC neural activity pattern (Experiments 1 and 2). Experiment 3 tested tools composed of two parts to understand better how grasping manner was computed from object visual inputs. Support vector machine analysis revealed that the LOTC activity could decode different shapes of the tools' handle parts but not the tools' head parts. Together, these results suggest that the LOTC parses tool shapes by how it maps onto grasping programs; such parsing is not fully based on the whole-object shape but rather an interaction between the whole (where to grasp) and its parts (distinguishing the shape for the grasping part for specific grasping manners).

1. Introduction

Being able to recognize and use manmade tools is a prominent feature of humans (Gibson et al., 1994; Tomasello, 1999). Brain imaging and lesion studies have found several brain areas in the temporal, parietal and frontal cortices that are preferentially involved in tool processing relative to other object domains, such as animals or faces, including a region in the left lateral occipitotemporal cortex (LOTC) in the ventral visual pathway (Chao et al., 1999; Lewis, 2006; Martin, 2007). Given that tools are made by humans to be grasped and manipulated for particular functions, their shapes are usually formed in a way that provides such motoric affordance. It has been commonly hypothesized that preferential activity to tools in this region might be related to such rich motor/action properties (Gallivan et al., 2013; Monaco et al., 2014; Perini et al., 2014; Wurm et al., 2017) or the specific shape representations with close connections with or even constrained by motor/action properties (Bi et al., 2016; J. Chen et al., 2017). The exact mechanisms in which visual inputs are translated into action properties for tool use, and the role of LOTC in this process, remain to be articulated and tested. The answer to these questions helps understand not only how tool information is represented but also how visual processing interfaces with other types of information in general.

Recent studies examined multiple types of shape- and action-related information in the LOTC. The results revealed positive effects of whole-object-level tool shape (Peelen and Caramazza, 2012; Bracci et al., 2017; Wang et al., 2018), elongation shape (Fabbri et al., 2016; J. Chen et al., 2017), grasping manner (Fabbri et al., 2016), with no consistent positive effects of "manner of manipulation" for functional use (Peelen and Caramazza, 2012; Wang et al., 2018; but see Bracci et al., 2017). Given the correlational nature between object shape and grasping manner, it has been difficult to examine whether these observed effects were attributed to either or both types of dimensions in this region. We do not know which shape representation level(s) (whole object shape vs. object parts) that motor/action properties connect with and/or constrain

* Corresponding author. State Key Laboratory of Cognitive Neuroscience and Learning & IDG/McGovern Institute for Brain Research, Beijing Normal University, Beijing, 100875, China.
** Corresponding author. State Key Laboratory of Cognitive Neuroscience and Learning & IDG/McGovern Institute for Brain Research, Beijing Normal University, Beijing, 100875, China.
E-mail addresses: wangxiaoying@mail.bnu.edu.cn (X. Wang), ybi@bnu.edu.cn (Y. Bi).

https://doi.org/10.1016/j.neuropsychologia.2020.107340
Received 20 August 2019; Received in revised form 26 November 2019; Accepted 10 January 2020
Available online 11 January 2020

either. The object processing literature showed that a brain area just posterior to the LOTC—the lateral occipital cortex (LOC)—tended to code object shapes in a nonholistic, part-based format (Guggenmos et al., 2015; Erdogan et al., 2016). Thus, it is possible that for tools with complex shapes, they are parsed into different object "parts", and the mapping to motoric manners (either manipulation or grasping manner) is based on these parts rather than the "holistic" shape of the whole object.

Here, in three experiments, we test these potential candidate representations in the LOTC that are relevant in the process of mapping a visual object with its action programs: the part shape, the whole-object shape, and the action-related features to which visual inputs are supposed to map onto. In Experiment 1 and 2, we combined representational similarity analysis (RSA) (Kriegeskorte et al., 2008a) and commonality analyses (Seibold and McPhee, 1979) to test both the unique and correlated contributions of whole object shape and action properties (manipulation or grasping for pickup). Grasping for pickup was shown to have the most significant explanatory power of the LOTC activation pattern across the first two experiments. Experiment 3 was designed to understand further how the grasping manner is computed based on visual input, if not by whole-object shape, by examining the hypothesis of a part-based shape-motor correspondence representation here. A set of tools that were conceived as having two clear parts (one elongated and one stubby) were selected to build an orthogonal design with tool part shape type (elongated or stubby) and part motor type ('handle' or 'head'), with the whole-object shape being roughly similar. If the LOTC actually represents object part-shapes that correspond to various grasping manners, it should not matter whether the part serves as a handle or a head in an object; alternatively, if some aspects of the grasping information is also computed based on whole-object shape (e.g., which part is up for grasping), the part's role in the whole object would also matter.

2. Experiment 1

The neural data of Experiment 1 were taken from a previous study (Peelen et al., 2014), which tested for brain regions that represented object shape knowledge independently of the input modality. In the current study, we collected additional behavioral ratings of the stimuli and combined with the neural data of the sighted subject group viewing pictures in that experiment, to test the candidate hypotheses about the representation in the LOTC-tool.

2.1. Materials and methods

2.1.1. Participants

We collected data from 15 subjects (7 female, aged 26–60), the data from three of the subjects were discarded from the following analyses because of excessive head motion (head motion > 3 mm or 3°). Subjects were in good health with no past history of psychiatric or neurological diseases and had normal or corrected-to-normal vision. They were compensated for their participation and gave informed consent to the experimental protocol approved by the institutional review board of Beijing Normal University (BNU) Imaging Center for Brain Research. A group of college students who did not take part in the fMRI experiment were recruited to rate the pairwise shape (N = 14) or motor similarity (grasping (N = 21) or manipulation manner (N = 22)) of the stimuli objects based on object names.

2.1.2. Materials

The stimuli were black-and-white photographs of 33 everyday household artifacts (see Fig. 1B for examples and Appendix for the whole list), each having three different exemplars.

2.1.3. Behavioral representational similarity matrix (RSM) construction

To construct behavioral RSMs, the stimuli were rated via an online survey with a 7-point scale (7 for most similar) (http://www.wjx.cn) on the following dimensions: (1) *Object shape similarity*. Participants were asked to rate "how similar in shape are the objects denoted by these two words?" Some examples of highly similar pairs (based on group-average data) on the shape dimension were balloon–ball (6.3) and chopsticks-straw (6.1). (2) *Object motor information similarity*. Two dimensions were examined. For the manipulation manner similarity, participants were presented with word pairs and asked to rate: "how similar in manipulation manner are the objects denoted by these two words; that is, how similar are the hand actions when you use these objects?" Some examples of highly similar pairs (based on group-average data) on the manipulation manner dimension were comb–toothbrush (4.2) and mask–glasses (4.7). For the grasping manner similarity, participants were presented the same word pairs and asked to rate: "how similar in grasping manner are the objects denoted by these two words; that is, how similar are the hand actions when you pick these objects up?" Some examples of highly similar pairs (based on group-average data) on the grasping manner dimension were ruler–comb (5.8) and nail–button (5.8). These two dimensions roughly corresponded to the actions for functional use versus for nonfunctional grasping. For these similarity ratings, participants were told to focus on the dimension of interest while disregarding other properties of the objects such as their real-world size, color, or tactile properties. This resulted in 3 group-average symmetric matrices of similarity based on shape, manipulation manner, and grasping manner. The inter-rater reliability for each rating was high (intra-class coefficients (ICC) of shape: 0.89, ICC of manipulation manner: 0.79, ICC of grasping manner: 0.87).

2.1.4. fMRI experimental procedure

Participants viewed trials of black-and-white photographs (800-ms picture presentation followed by 1200-ms fixation) and were instructed to press one of two buttons by comparing the real-world size of each object with that of a typical adult's hand palm (object-size judgment task) (Fig. 1C). Each run consisted of 99 2-s-long picture trials and 33 2-s-long fixation trials and started and ended with a 12-s fixation. Trial order was pseudo-randomized with the restriction that no two consecutive objects were identical and that both the first and the last presentation were picture trials. Each of the 33 object conditions was presented three times within a run, with each exemplar presented once. The whole session consisted of five runs, each lasting 4 min and 48 s, resulting in 15 presentations per object across the whole experiment.

2.1.5. Definition of regions of interest (ROI)

The tool-preferring left LOTC (Fig. 1A) was obtained using data from an independent study (Wang et al., 2016), which included grayscale images from four object domains (tools, animals, scenes and neutral faces) in a block design. Contrasting responses to tools to the average responses to the other three object domains yielded a left LOTC cluster (one-tailed $P < 0.0001$, uncorrected, with peak Montreal Neurological Institute (MNI) coordinates xyz: −51, −66, −3), which closely corresponds to previous studies in the literature (the peak coordinates in Mahon et al., 2007 is xyz: −49, −61, −7, Talairach space; the mean coordinates in Bracci et al., 2012 is xyz: −48 −65, −6, Talairach space). This ROI (Fig. 1A) was transformed from the MNI space into the Talairach space for Experiment 1 (peak MNI coordinates xyz: −51, −66, −3; corresponding Talairach coordinates xyz: −48, −63, −5) using the "icbm2tal" transformation (Lancaster et al., 2007).

2.1.6. Data acquisition and preprocessing

All functional and structural MRI data were acquired with a 3T Siemens Trio Tim scanner at the BNU MRI center. A high-resolution 3D structural dataset was collected with a 3D-MPRAGE sequence in the sagittal plane (144 slices; repetition time (TR) = 2530 ms; echo time (TE) = 3.39 ms; flip angle = 7°; matrix size = 256 × 256; voxel size = 1.33 × 1 × 1.33 mm). BOLD activity was measured with an echo-planar imaging (EPI) sequence (TR = 2000 ms; TE = 30 ms; flip angle = 90°;

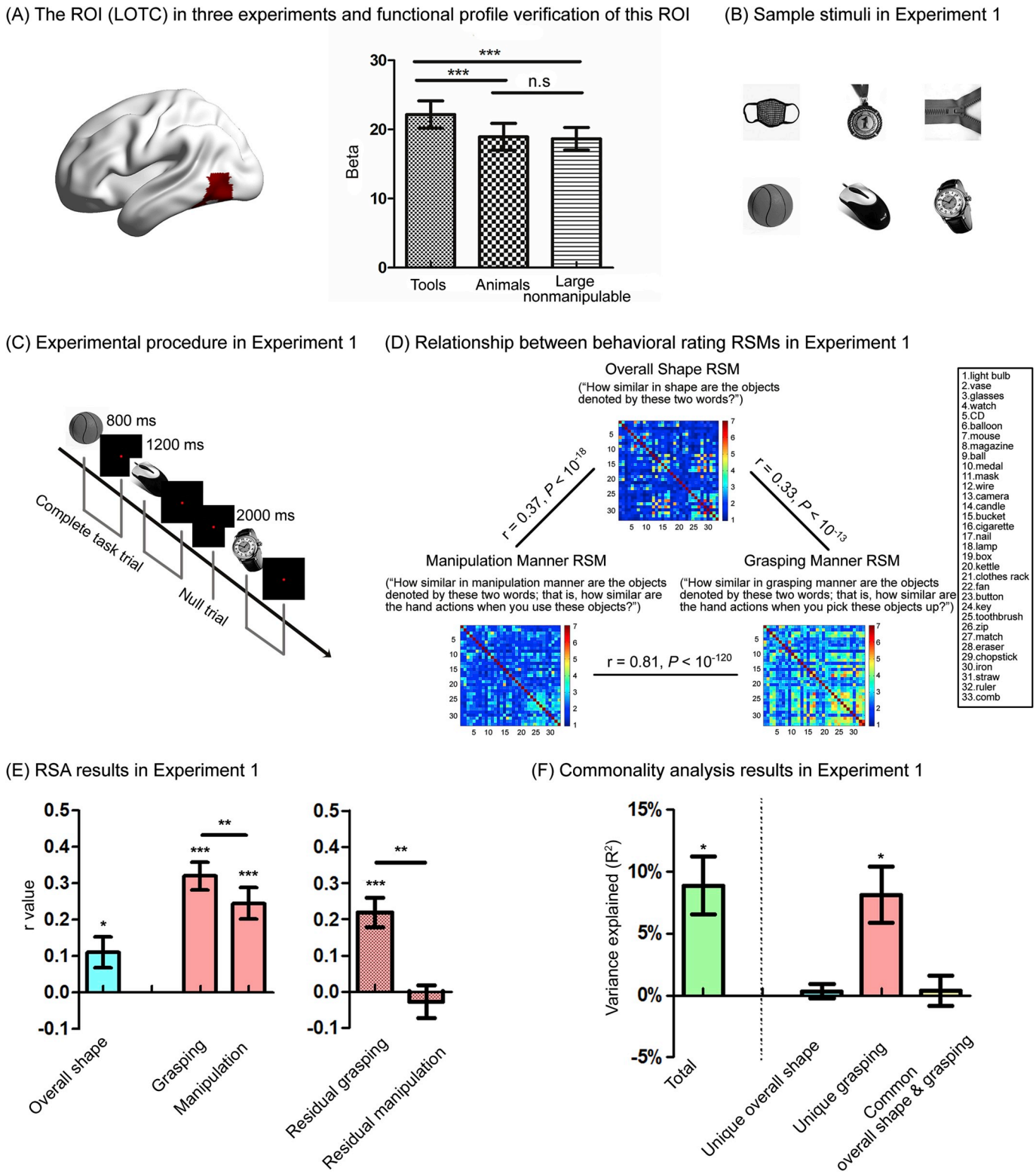

Fig. 1. Predefined ROI (LOTC) and ROI-based analysis results in Experiment 1. **(A)** The ROI (LOTC) used in the three experiments, which was obtained using data from a previous study (Wang et al., 2016). The bar plot shows this LOTC ROI's activation (Beta) to each stimulus domain (tools, animals, large nonmanipulable objects) in Experiment 2. Error bars indicate standard error of the mean (SEM). **(B)** Sample stimuli in Experiment 1 (mostly small manipulable everyday objects). **(C)** Experimental procedure in Experiment 1. **(D)** The behavioral RSMs of overall shape, manipulation manner and grasping manner and the correlation between them. **(E)** The RSA results of overall shape, manipulation manner and grasping manner computed using raw correlations **(left)** and part correlations (**right**, regressing out one action information from the other). The asterisk over each bar indicates the significance level of the correlation coefficient; $^{*}P < 0.05$, $^{**}P < 0.01$, $^{***}P < 0.001$ (Bonferroni corrected, one-tailed). The asterisk between 2 bars indicates the significance level of Hotelling's *t*-test between the 2 bars; $^{*}P < 0.05$, $^{**}P < 0.01$, $^{***}P < 0.001$ (two-tailed). Error bars were SEM determined by bootstrap estimation (10,000 iterations). **(F)** The bar plot shows the variance partition computed from the commonality analysis. The asterisk over each bar indicates the significance level, which was decided by the percentile-based 95% two-tailed confidence intervals produced by bootstrap estimation (10,000 iterations). Error bars were SEM determined by bootstrap estimation (10,000 iterations).

matrix size = 64 × 64; voxel size = 3 × 3 × 3.5 mm with gap of 0.7 mm, 33 axial slices). fMRI preprocessing and analysis were performed using BrainVoyager QX v2.3. The first five volumes (10 s) of each run were discarded. Preprocessing of the functional data included slice time correction, 3D motion correction, and high-pass filtering. No spatial smoothing was applied. For each participant, the functional data were then registered to her/his anatomical data and transformed into Talairach space. The functional data were analyzed using the general linear model (GLM). Thirty-three regressors of interest corresponding to the 33 objects and six regressors of no interest corresponding to the six motion parameters were included.

2.1.7. Representational similarity analysis (RSA)

To build the neural RSM of the left LOTC, we calculated the Pearson correlation of multivoxel response patterns (for each voxel: t values relative to baseline) in our mask for each pair of stimuli, resulting in an individual symmetric RSM for each participant. These individual neural RSMs were then Fisher transformed and averaged across participants to obtain a group-average neural RSM. Then, we computed the Spearman correlations between the group-average neural matrix and the subjectively rated object similarity matrices for various object information dimensions. To determine which might be the effective action dimension represented in the LOTC, we also computed part correlations between the neural similarity matrix and the residual rating matrices for the two motor-related properties by regressing out one motoric variate (e.g., manipulation manner) from the other (e.g., grasping manner). The error bars of the correlation values between the neural and behavioral RSMs were determined using bootstrap resampling (10,000 iterations) (Efron and Tibshirani, 1994; Kriegeskorte et al., 2008b). The bootstrap results simulated a distribution of the correlation values, which allows us to obtain error bars on the arbitrary RSM statistics: the standard deviation of the bootstrap distribution is the standard error of the estimate of the statistic. In addition to the analyses performed on the group-average neural RSM, we also performed statistical analyses based on individual participant correlations, allowing for population-level inferences. For each participant, the correlations between neural similarity matrix and the behavioral rating similarity matrices were computed and Fisher-z transformed. To test for significance, correlations were tested against zero using one-sample t-tests.

2.1.8. Commonality analysis

Given the potential intercorrelations among the cognitive variables (shape, grasp), we further employed the commonality analysis method (Seibold and McPhee, 1979; Nimon et al., 2008; Kraha et al., 2012; Nimon and Oswald, 2013) to uncover the unique versus common contributions of multiple cognitive variables in explaining the variances in the neural RSM (see Greene et al., 2016; Bonner and Epstein, 2018; Hebart et al., 2018, for a similar approach using multiple model RSMs). Specifically, commonality analysis is a variance partitioning procedure that allows decomposing the model fit (R^2) into nonoverlapping uniquely and commonly explained partitions. Unique partitions represent the contributions of every single predictor above the other predictors in explaining the outcome variables, and they are mathematically equal to incremental R^2 and squared semipartial correlations. Common partitions measure the variance in common accounted for by two or more predictors. In our study, we adopted bootstrap estimation (10,000 iterations) to calculate the standard error of each partition, and the percentile-based 95% two-tailed confidence intervals produced by the bootstrap estimation were used to determine the significance of each partition. It is worth noting that, unlike unique partitions, the common partitions may assume both positive and negative values, with the latter allowing us to recognize the presence of suppressor predictor variables (Pedzahur, 1997; Capraro and Capraro, 2001; Kraha et al., 2012). The commonality analysis was calculated using the R software (www.R-project.org) with the "yhat" package (Nimon et al., 2013).

2.2. Results

2.2.1. Relationship between behavioral rating information dimensions

Three different RSMs across all pairs of 33 small artifacts were constructed based on the behavioral ratings (see Materials and Procedure). To examine relations among these behavioral RSMs, the Spearman correlations between each of them were computed (Fig. 1D). The *overall shape* RSM was correlated with the *grasping manner* RSM (r = 0.33, one-tailed $P < 10^{-13}$) and the *manipulation manner* RSM (r = 0.37, one-tailed $P < 10^{-18}$). The correlation value between the *manner of manipulating* and *manner of grasping* RSMs was also significant (r = 0.81, one-tailed $P < 10^{-120}$) (all Bonferroni corrected). These results show that the overall shapes of the tools were correlated with the manners of grasping as well as manipulating these tools.

2.2.2. The RSA results in the LOTC

We used RSA and commonality analysis to test whether the LOTC represents the overall tool shape, the tool motor information or a tight mapping between the shape and motor information of tools. We computed the Spearman correlations between the LOTC neural RSM and the three behavioral RSMs (Fig. 1E). The *overall tool shape* RSM was significantly correlated with the neural RSM of the LOTC (r = 0.11, one-tailed $P < 0.05$). Both the *grasping manner* RSM (r = 0.32, one-tailed $P < 10^{-13}$) and *manipulation manner* RSM (r = 0.24, one-tailed $P < 10^{-7}$) were significantly correlated with the LOTC neural RSM (all Bonferroni corrected). The effect of the *grasping manner* was significantly greater than the effect of the manipulation manner (Hotelling's *t*-test: $t_{(525)} = 3.14$, two-tailed $P < 0.01$). We also performed a part correlation between the neural similarity matrix and residual rating matrices for the two motor-related properties by regressing out one motoric variate (e.g., manipulation manner) from the other (e.g., grasping manner). The results showed that after regressing out the effect of the manipulation manner, *grasping* was still significantly correlated with the neural pattern of the LOTC (r = 0.22, one-tailed $P < 10^{-6}$), while the reverse was not true for the *manipulation manner* (r = −0.03, one-tailed $P = 0.74$) (all Bonferroni corrected). The effect of the *residual grasping manner* was significantly greater than the effect of the *residual manipulation manner* (Hotelling's *t*-test: $t_{(525)} = 3.21$, two-tailed $P < 0.01$). Note that we have also run significance testing using permutation tests (10,000 iterations) on the RSMs by computing correlations between the neural pattern and behavioral RSMs after randomly shuffling the labels of the stimuli. This yielded, for each comparison, a probability of obtaining a correlation under the null hypothesis that was the same or larger as those obtained between the original matrices. Similar patterns of results were obtained (Supplementary Table S1). The statistical analyses based on individual participant correlations yielded largely similar results (Supplementary Figure S1A).

2.2.3. The commonality analysis results in the LOTC

Considering the dominant effect of grasping over manipulation manner and the complexity of interpreting the commonality results caused by adding more variates, we first considered only the grasping manner as the information related to motoric pattern mapping. To disentangle the unique contribution of the overall shape property, the unique grasping information, and the shared information between these two dimensions (i.e., the grasping variation that is fully correlated with the shape variation), we conducted a commonality analysis to break down the neural pattern variances explained by these three portions. As shown in Fig. 1F, the commonality analyses revealed that the *overall tool shape* and *grasping manner* together explained 8.88% of the variance in the neural RSM, and the unique effects of *grasping manner* (i.e., uncorrelated with the *overall tool shape)* contributed to 91.67% of this explanatory power (8.14% of the variance in the neural RSM, $P < 0.05$); the *common variance* in the shape and grasping manner and the unique contribution of the *overall tool shape* was negligible (together contributed to 0.74% of the variance in the neural RSM). The results showed

that information uniquely related to the manner of grasping was encoded by the LOTC. The significance and error bars were determined by bootstrap estimation (10,000 iterations) using the "yhat" 2.0 package (Nimon et al., 2013).

We also conducted commonality analysis with all three models (overall shape, grasping and manipulation) as a validation, which also revealed unique grasping as the only significant partition that contributes to the neural pattern variances of the LOTC (Supplementary Figure S2A).

3. Experiment 2

The purpose of the second experiment was to replicate the results in Experiment 1 using more strictly defined tools, given that in Experiment 1, we did not distinguish between strictly defined tools and other small manipulable objects (e.g., candle), which may be differentially represented in the LOTC (see discussions in Mahon et al., 2007). In this experiment, we computed the RSA and commonality analysis using items that were strictly defined as "tools" (following Mahon et al., 2007), which were manipulable objects that have systematic relationships between their physical form and their manner of manipulation/function (e.g., hammer, scissors, wrench).

3.1. Materials and methods

3.1.1. Participants

Twenty-nine subjects (19 female, aged 19–33) who did not take part in Experiment 1 participated in this experiment, and three of the subjects were excluded because of excessive head motion (head motion > 2 mm or 2°). Subjects were in good health with no past history of psychiatric or neurological diseases and had normal or corrected-to-normal vision. They were compensated for their participation and gave informed consent to the experimental protocol approved by the institutional review board of BNU Imaging Center for Brain Research. Another group of healthy subjects (N = 22, college students) participated in the behavioral ratings of the similarities in shape, manipulation manner and grasping manner following the identical procedures to those of the rating experiments of Experiment 1. The college student participants were also asked to rate the handle shape similarity of the materials. They were presented with word pairs and asked to rate: "how similar are the shapes of tool parts that you contact with when you pick these objects up for using?" The inter-rater reliability for each rating was high (ICC of shape: 0.92, ICC of manipulation manner: 0.92, ICC of grasping manner: 0.95, ICC of handle shape: 0.93).

3.1.2. Materials

The data set of this experiment included 95 colored photographs from various object domains, including animals (N = 32), small manipulable objects (N = 35), and large nonmanipulable objects (N = 28). For the current purpose, we only focused on a subset of strictly defined "tools" (N = 15; selection criterion following Mahon et al., 2007, see Fig. 2A for example stimuli and Appendix for the whole list).

3.1.3. fMRI experimental procedure

There were six runs lasting 8 min and 48 s each. Each run consisted of 95 picture trials (500-ms fixation followed by 800-ms picture presentation and 2700-ms blank screen) presented exactly once and 64 2-s-long interspersed null trials, the orders of the trials were randomized using "optseq" (http://surfer.nmr.mgh.harvard.edu/optseq/) (Fig. 2B). Additionally, five 2-s-long null trials were placed at both the beginning and the end of each run. The participants were instructed to speak out the corresponding item's name in each picture trial.

3.1.4. Data acquisition and preprocessing

Imaging data were acquired with a 3 T S Trio Tim scanner at the BNU MRI center with the same scanning parameters in Experiment 1. The imaging data were preprocessed using Statistical Parametric Mapping software (SPM12; Wellcome Trust Center for Neuroimaging, http://www.fil.ion.ucl.ac.uk/spm/software/spm12/) and MATLAB. The functional image preprocessing procedure was identical to that used in Experiment 1, except that the images were normalized into the MNI space using unified segmentation. The functional data were analyzed using the GLM. For the main analyses in Experiment 2, ninety-five regressors of interest corresponding to the 95 objects and six regressors of no interest corresponding to the six motion parameters were included.

The ROI in Experiment 2 was the same as that used in Experiment 1 (i.e. adopting from Wang et al., 2016), without the transformation from the MNI space into the Talairach space. The inclusion of both tool and other domains (animals and large nonmanipulable objects) in Experiment 2 allowed us to further verify that the ROI we used indeed showed tool preferences in the current experiment. We built a GLM that included 4 predictors corresponding to the strictly defined tool, other small manipulable object, animal and large nonmanipulable object domains, along with 6 head motion parameters as covariates of no interest. Within the LOTC ROI, we extracted the activity signals of tools and compared it with the activities to animals and large nonmanipulable objects across all participants with paired-sample t-tests. The results (Fig. 1A, bar plot) confirmed stronger responses for tools in this area than both animals (paired-sample *t*-test: $t_{(25)} = 3.97$, one-tailed $P < 0.001$, Cohen's d = 0.78) and large nonmanipulable objects (paired-sample *t*-test: $t_{(25)} = 4.75$, one-tailed $P < 0.001$, Cohen's d = 0.93) (all Bonferroni corrected). The tool selectivity effect size found in this validation analysis was comparable with previous studies (for instance, in Bracci et al., 2012, tool > animals, $t_{(13)} = 4.97$, $P < 0.001$, Cohen's d = 1.33; in Bracci et al., 2016, tools > large nonmanipulable objects, $t_{(14)} = 3.75$, $P < 0.001$, Cohen's d = 0.97). The methods of the ROI-based RSA and commonality analysis in Experiment 2 were the same as those used in Experiment 1.

3.2. Results

3.2.1. Relationship between behavioral rating information dimensions

The behavioral rating RSMs for overall tool shape, grasping manner, and manipulation manner are shown in Fig. 2C. The *overall shape* RSM was correlated with the *grasping manner* RSM (r = 0.49, one-tailed $P < 10^{-6}$) and the *manipulation manner* RSM (r = 0.55, one-tailed $P < 10^{-8}$). The correlation value between the *manner of manipulating* and *manner of grasping* was also highly significant (r = 0.90, one-tailed $P < 10^{-37}$) (all Bonferroni corrected, Spearman correlation). While the behavioral RSM correlation results are similar in overall pattern to those of Experiment 1, the magnitude of the associations between manipulation with overall tool shape and grasping were stronger in this experiment (Fisher's Z-test: $Zs > 2.13$, two-tailed $ps < 0.05$), likely due to the nature of the stimuli used here (strictly defined tools versus general manmade artifacts).

3.2.2. The RSA results in the LOTC

The RSA results in the LOTC in Experiment 2 are shown in Fig. 2D. The *grasping manner* RSM (r = 0.26, one-tailed $P < 0.05$; all Bonferroni corrected) was significantly correlated with the LOTC neural RSM. The *manipulation manner* RSM (r = 0.16, one-tailed $P = 0.16$) showed a trend of a correlation with the LOTC neural RSM. The *overall tool shape* RSM did not show any effects (r = 0.07, one-tailed $P = 0.68$), probably because the stimuli set, being typical tools, tended to have elongated overall shapes without sufficient variance (for shape RSM in Experiment 2, mean similarity = 3.18, standard deviation (SD) = 1.00, coefficient of variation (CV) = 0.32; for shape RSM in Experiment 1, mean similarity = 2.05, SD = 0.96, CV = 0.47). The effect of *grasping manner* was significantly greater than that of *manipulation manner* (Hotelling's *t*-test: $t_{(102)} = 2.48$, two-tailed $P < 0.05$). As in Experiment 1, after regressing out one motoric variate from the other, the grasping manner was still significantly correlated with the neural pattern of the LOTC (r = 0.35, one-tailed $P < 0.001$), but the manipulation manner was not (r = −0.25, one-tailed $P = 1$) (all Bonferroni corrected). The effect of the *residual*

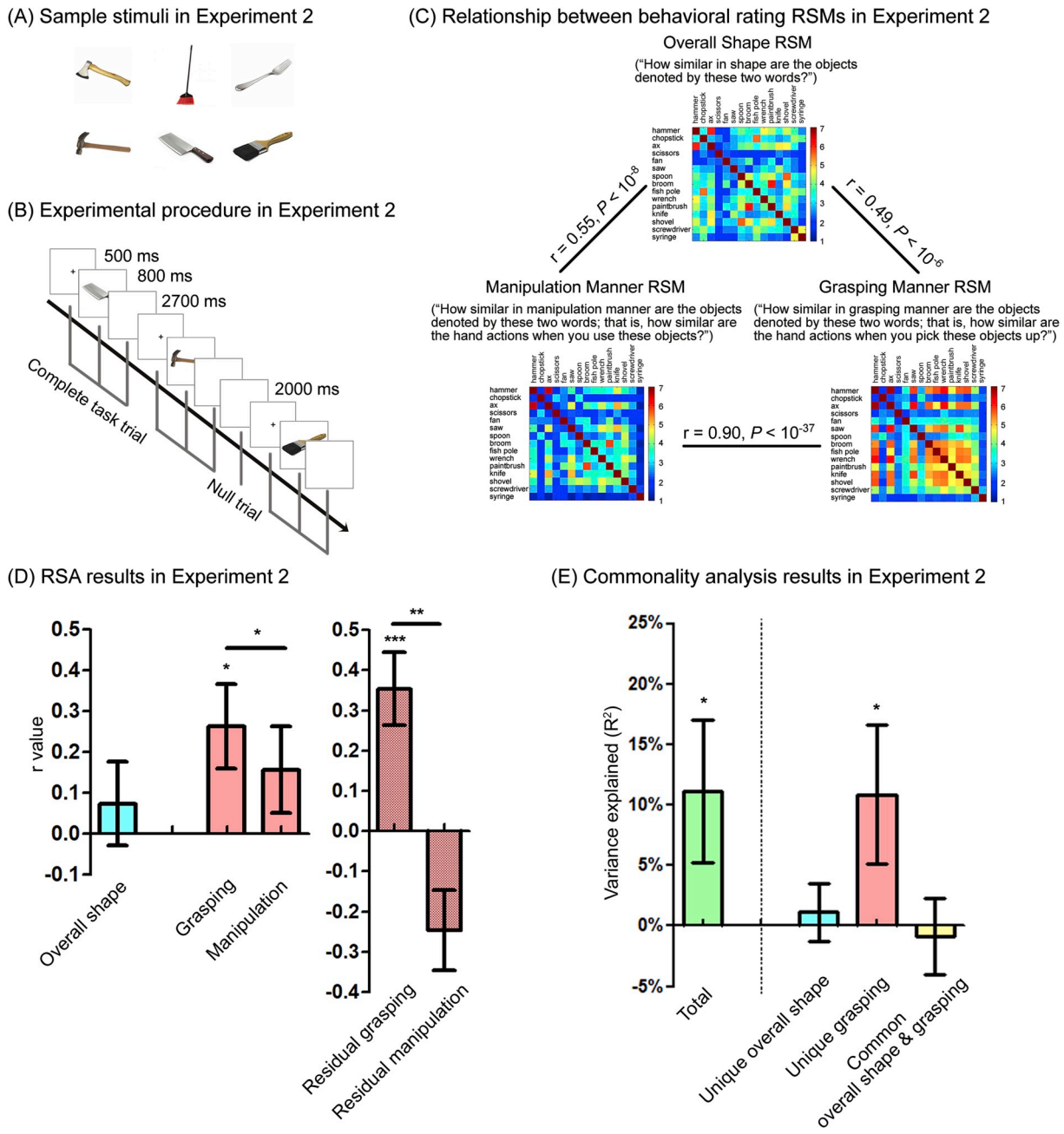

Fig. 2. ROI-based analysis results in Experiment 2. **(A)** Sample stimuli in Experiment 2 (typical tools). **(B)** The experimental procedure in Experiment 2. **(C)** The behavioral RSMs corresponding to different object information dimensions and the correlations between them. **(D)** The ROI-based RSA results computed using raw correlations **(left)** and part correlations (**right,** regressing out one action information from the other). The asterisk over each bar indicates the significance level of the correlation coefficient; $*P < 0.05$, $**P < 0.01$, $***P < 0.001$ (Bonferroni corrected, one-tailed). The asterisk between 2 bars indicates the significance level of Hotelling's *t*-test between these 2 bars; $*P < 0.05$, $**P < 0.01$, $***P < 0.001$ (two-tailed). Error bars were SEM determined by bootstrap estimation (10,000 iterations). **(E)** The bar plot of variance decomposition in the LOTC. The asterisk over each partition indicates the significance level, which was decided by the percentile-based 95% two-tailed confidence intervals produced by bootstrap estimation (10,000 iterations). Error bars were SEM determined by bootstrap estimation (10,000 iterations).

grasping manner was significantly greater than the effect of the *residual manipulation manner* (Hotelling's *t*-test: $t_{(102)} = 3.38$, two-tailed $P < 0.01$). Note that we also ran significance testing using permutation tests (10,000 iterations) on the RSMs, and similar patterns of results were obtained (Supplementary Table S1). We also conducted statistical analyses based on individual participant correlations, allowing for population-level inferences, and these analyses provided similar results (Supplementary Figure S1B).

3.2.3. The commonality analysis results in the LOTC

We still performed the commonality analysis to visualize the effects of shape and grasping and their potential correlated variances in explaining the neural pattern variances. The results (Fig. 2E) revealed that the *overall tool shape* and *grasping manner* together explained 11.15% of the variance in the neural RSM, and the unique effects of *grasping manner,* which was uncorrelated with *overall tool shape*, contributed to 97.49% of this explanatory power (10.87% of the variance in the neural RSM, $P < 0.05$); the *common variance* in the overall shape and grasping manner, and the unique contribution of *overall tool*

shape to the explanatory power were negligible (together contributed to 0.28% of the variance in the neural RSM). The results again showed that information uniquely related to grasping manners was encoded by the LOTC. The significance and error bars were determined by bootstrap estimation (10,000 iterations) using the "yhat" 2.0 package. Like in Experiment 1, we conducted commonality analysis with all three models (overall shape, grasping and manipulation) and the results also suggested that the unique grasping is the only significant partition that contributes to the neural pattern variances of the LOTC (Supplementary Figure S2B). Besides, given the shape of specific exemplar was presented in Experiment 2 (only one exemplar for each object), we also ran the RSA and commonality analysis with behavioral models rated in images in this experiment (rating from another group of college students, N = 20), the result pattern remained similar (Supplementary Figure S3).

The commonality analysis results in both Experiment 1&2 showed that the neural pattern of the LOTC encodes information related to the manner of grasping, and intriguingly, not the grasping manner computed from overall object shapes—the effect of shared components between the grasping manner and overall shape was not significant. Considering grasping manner is more likely computed from tool handle's shape rather than the overall shape of the tool, we tested whether the grasping manner effect is associated with handle shapes more specifically. Given that most objects in Experiment 2 had clear handle or head parts, we collected the handle part shape rating for the objects in Experiment 2 and performed commonality analysis with grasping and handle part shape (instead of the overall object shape above). The results showed that the *common variance* shared by handle part shape and grasping contributed the most to the neural pattern variance of the LOTC (7.73% of the variance in the neural RSM, $P < 0.05$), and the *unique tool handle shape* and the *unique grasping manner* only contribute to 2.32% of the LOTC neural pattern variance in total. These results indicated an object-part-based representation in the LOTC.

4. Experiment 3

In this experiment, we further explored whether the LOTC's grasping manner effects is computed from object part shapes. We selected a set of tools that are typically considered as having two parts (one elongated and one stubby) to build an orthogonal design with tool part shape (elongated or stubby) and tool part type ('handle' or 'head'), with the whole-object shape being roughly similar. If the LOTC represents only object part-shapes that correspond to various grasping manners, it should not matter whether the part serves as a handle or a head in an object; alternatively, if some aspects of the grasping information is also computed based on whole-object shape (e.g., which part is up for grasping), the part's role in the whole object would also matter.

4.1. Materials and methods

4.1.1. Participants

Twenty-five subjects participated (15 female, aged 18–26) in this experiment. Subjects were in good health with no past history of psychiatric or neurological diseases and had normal or corrected-to-normal vision. They were compensated for their participation and gave informed consent to the experimental protocol approved by the Human Subject Review Committee at Peking University. Another group of college students (N = 35) rated the similarity of the perceptual shape of the tools and tool parts (N = 23) or the familiarity with the tools (N = 12).

4.1.2. Materials

We collected black-and-white photographs of eight integrated tools that had obvious handle-head binary components (see Fig. 3A), with

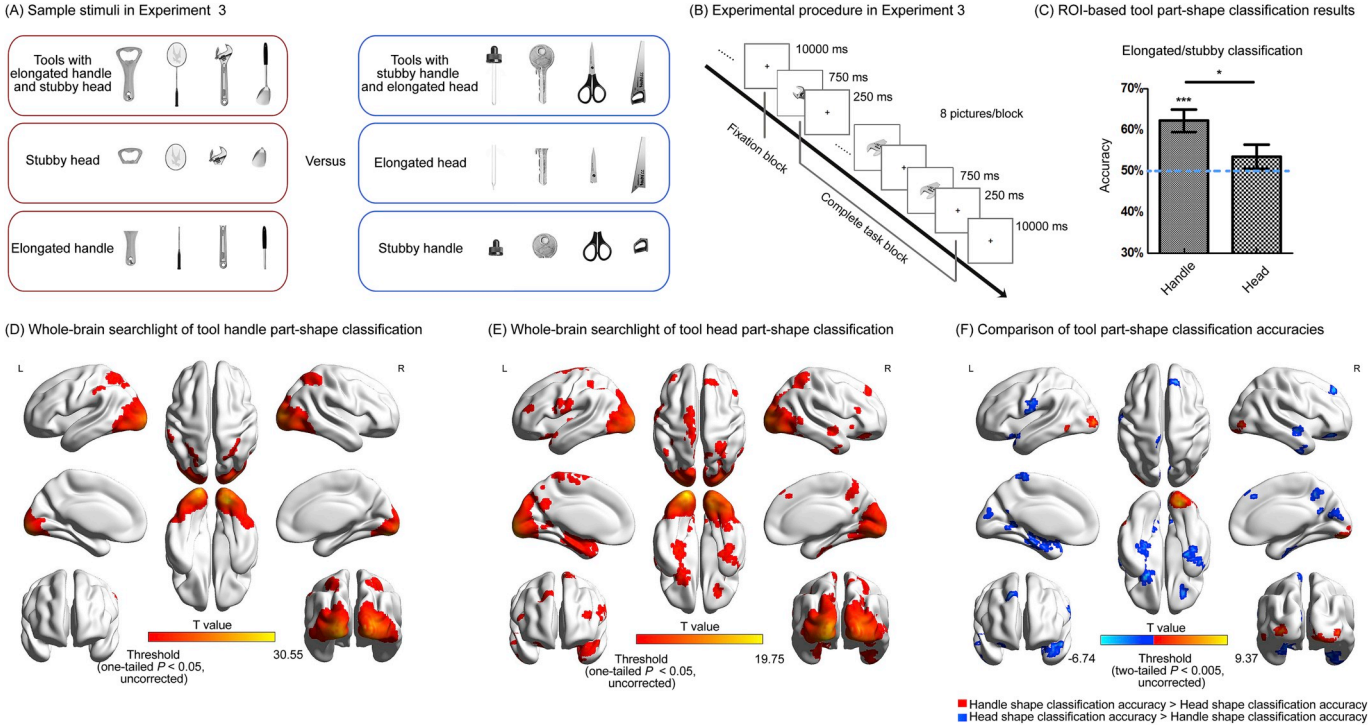

Fig. 3. SVM analysis results in Experiment 3. **(A)** The stimulus exemplars that used in Experiment 3. **(B)** The experimental procedure in Experiment 3. **(C)** ROI-based SVM analysis results in Experiment 3. The asterisk over each bar indicates the significance level of classification accuracy. $*P < 0.05$, $**P < 0.01$, $***P < 0.001$ (Bonferroni corrected, one-tailed). Chance level is 50% (dashed line). Error bars denote SEM. The asterisk between 2 bars indicates the significance level of the paired-sample *t*-test between the 2 bars; $*P < 0.05$ (two-tailed). **(D) (E)** Whole-brain part-shape searchlight SVM results in Experiment 3. The searchlight was performed for handles/heads separately. Threshold at one-tailed $P < 0.05$, uncorrected, cluster size ≥ 10. **(F)** Comparison between handle-shape classification accuracy and head-shape classification accuracy. The paired-sample *t*-test was conducted within the combined areas in Fig. 3D and E to ensure that the comparison results were not elicited by two classification accuracies lower than chance level (50%). Threshold at two-tailed $P < 0.005$, uncorrected, cluster size ≥ 15.

eight different exemplars across different directions for each tool. We then obtained the tool part stimuli by splitting the original pictures into two parts: tool handles (graspable parts) and heads (functional parts).

4.1.3. Potential confounding variates measurement

To test whether the results we found were driven by confounding variates, we collected behavioral data of different perceptual and visual information. The perceptual shape similarity of each pair of items from the same item group (integrated tools, tool handles, or tool heads) was collected online (http://www.wjx.cn). For each item group, all exemplars (eight for each item) from this group were first shown at the top of the corresponding questionnaire for subjects to become familiar with the items. Then, the bottom of the questionnaire presented pairs of tool names, and the participants were asked to rate the shape similarity of each pair on a 7-point scale (7 for most similar): "how similar in shape are the tools (or handle/head of the tools) denoted by these words?" The representational matrices of gist dissimilarity (Oliva and Torralba, 2001) and pixel similarity were calculated using all the exemplars across all item groups from the fMRI experiment with MATLAB R2012a code. The familiarity of each integrated tool was also rated online using a 7-point scale (7 for most familiar) in case the tools from different conditions were confounded with familiarity differences.

4.1.4. fMRI experimental procedure

During fMRI scanning, subjects participated in six 7-min-24-s runs, and each run contained one block of each of the eight tool stimuli and corresponding tool parts, for a total of 24 blocks (eight whole tool blocks, eight handle blocks, and eight head blocks) per run (Fig. 3B). Each block lasted 8 s, which included eight 1-s picture trials (750-ms picture presentation followed by 250-ms fixation for each trial), and the blocks were separated by 10-s fixation periods. Stimulus pictures in the same block represented several distinct exemplars of the same tool or tool part, except for the adjacent repeated images. A 10-s-long and a 12-s-long fixation trial were included at the beginning and end of each run. Before the scanning session, all subjects were instructed to become familiar with the stimulus pictures, including both the integrated tools and tool parts. The task for all runs was a 1-back task in which subjects detected consecutive repetitions of the same image that occurred one or two times per block. The total number of repetitions was balanced for each item.

4.1.5. Data acquisition and preprocessing

The fMRI data were collected on a 3 T MAGNETOM Prisma MR scanner (Siemens, Erlangen, Germany) with a 64-channel head-neck coil at the Center for MRI Research, Peking University. High-resolution functional images were acquired using a multiband echo-planar sequence (TR = 2000 ms, TE = 30 ms, flip angle = 90°, field of view (FOV) = 224 mm × 224 mm, matrix size = 112 × 112, 62 axial slices, slice thickness = 2.0 mm, voxel size = 2 × 2 × 2 mm with gap of 0.3 mm, multiband factor = 2). High-resolution three-dimensional T1-weighted images were acquired using the magnetization-prepared rapid gradient-echo sequence (TR = 2530, TE = 2.98 ms, inversion time = 1100 ms, flip angle = 7°, FOV = 256 mm × 224 mm, matrix size = 224 × 256, interpolated to 448 × 512, 192 sagittal slices, slice thickness = 1.0 mm, voxel size = 0.5 × 0.5 × 1 mm). The images were preprocessed using SPM12. The first five volumes of each run were discarded, and each subject's anatomy was registered automatically to the MNI coordinate system. The functional image preprocessing procedure was identical to that in Experiment 2. Functional data were analyzed using the GLM. Twenty-four regressors of interest corresponding to the 24 items (integrated tools or tool parts) and six regressors of no interest corresponding to six motion parameters were included. The same LOTC ROI used in Experiments 1 and 2 was adopted in this experiment for the following analyses.

4.1.6. Support vector machine (SVM) analysis

This experiment was specifically designed for a two-category classification with part identity (handle vs head) and part shape (elongated vs stubby), where we tried to maximize between-condition variations and minimize the within-condition variation. We thus performed ROI-based linear SVM classification analyses for each subject, using the MATLAB LIBSVM library (Chang and Lin, 2011). To be specific, in the predefined ROI, for each item (tool part or whole tool), we summed the voxels' activation patterns from the six blocks corresponding to the identical item across six runs and acquired one activation pattern for each item. Then, stimulus labels were assigned to each item based on the information dimension we wanted to examine. The pixel intensity value of each stimulus picture was extracted based on the average gray level of the exemplars of the item and was regressed out from the voxel activation pattern across all stimuli before encoding. Scaling was conducted on neural patterns of training and testing data separately before applying SVM (Hsu et al., 2003).

LOTC decoding: Shape information within different types of tool parts. Two separate part-based classifiers were trained: one to discriminate different shapes (elongated vs. stubby) within the tool handle stimuli group and one to discriminate different shapes within the tool head group. For each classifier, we selected six tool parts for training and the left two tool parts for testing, and the training and testing processing was iterated 16 times so that every possible combination of training and testing set was considered. The results were averaged over all possible choices of validation iterations. We produced two decoding accuracies for each subject, and two one-sample t-tests compared with chance level (50%) were conducted to test significance.

LOTC decoding: The "grasping-role-in-tool" information. To test whether the LOTC can encode the "grasping-role-in-tool" information of a tool part for the handle-shape sensitivity to emerge, we conducted two additional ROI-based SVM analyses. One analysis attempted to find whether the LOTC was able to decode the role of a tool part (a handle or a head) based on the activation patterns associated with the tool part stimuli. For each subject, we selected seven pairs of tool parts for training and the remaining pair of tool parts from one integrated tool for testing (discriminating handle or head of this tool), and the training and testing processing was iterated eight times so that each pair of tool parts was equally considered in the testing set. We produced decoding accuracy for each subject by averaging the accuracies of all possible choices of validation iterations, and a one-sample *t*-test compared with chance level (50%) was conducted to test significance across all subjects. In this manner, a significantly successful classification indicates that the region could discriminate tool handle from tool head even the shape information varied hugely. We also conducted this part identity classification using split sets of stimuli to exclude the influences of shape on classification accuracy (decoding handle/head within elongated parts and stubby parts). Another ROI-based SVM tested whether the LOTC could discern whether a whole tool has an elongated handle or a stubby one. For each subject, we selected six tools (three tools with elongated handles and three with stubby ones) for training and the remaining two tools for testing, and the training and testing processing was iterated 16 times so that every possible combination of training and testing set was considered. Decoding accuracy for each subject was acquired by averaging the accuracies of all possible choices of validation iterations, and a one-sample *t*-test compared with chance level (50%) was conducted to test significance across all subjects.

Whole-brain searchlight: Decoding the shape information within different types of tool parts. We ran the tool part-shape decoding (elongated vs. stubby within tool handles and tool heads) in whole-brain searchlight analyses to test the other brain regions that are sensitive to handle or head shape information. For each voxel across the gray matter in the cerebral cortex, a sphere with a 12-mm radius that was centered on this voxel was created as an ROI, and decoding analyses that were identical to previous ROI-based SVM were performed for this ROI. The decoding accuracy was assigned to the central voxel. We produced two decoding

accuracy maps for each subject (decoding shapes within tool handles and tool heads). To test for significance for tool handles and tool heads respectively, two one-sample t-tests compared with chance level (50%) were conducted for each voxel in the brain across all subjects. We further compared the effect magnitude of shape-within-handle with the effect magnitude of shape-within-head in the combined areas that showed either handle shape or head shape decoding effects (one-tailed $P < 0.05$, uncorrected), by computing a paired-sample *t*-test on each voxel in the combined areas with the decoding accuracy maps across all subjects. The results are shown in the MNI space and projected onto the MNI brain surface using the BrainNet viewer (http://www.nitrc.org/projects/bnv/) (Xia et al., 2013).

4.1.7. RSA

While this experiment was designed specifically for a classification analysis, RSA with the same methods in Experiment 1 and 2 was still performed to present a full picture. Briefly, for each participant, we calculated the Pearson correlation of multivoxel response patterns (for each voxel: t values relative to baseline) in our mask for each pair of stimuli within the same item group (integrated tools, tool handles, or tool heads). These individual neural RSMs were then Fisher transformed, and three group-averaged neural RSMs of the left LOTC were built for the three item groups, respectively. Then the Spearman correlations between the group-average neural matrices and the subjectively rated tool (or tool part) shape similarity matrix were calculated.

4.2. Results

Experiment 3 tested whether the relationship between whole-object-based and part-based parsing of graspability. We carefully selected 8 typical tools that were composed of one graspable part ('handle') and a functional part ('head'), where the part shape (stubby vs. elongated) and type (handle vs. head) were orthogonally varied. If the LOTC processing was fully part-shape based, then it would be the shape/graspability of the parts that matters and not the whole object; if the grasping information about the whole object also matters, the role of the part within the whole object may matter (handle or head). We tested this by performing machine-learning-based decoding of various types of information of interest.

4.2.1. The part-shape decoding results in the LOTC

To examine whether the decoding of part shape information can be affected by different tool part types in the LOTC, we conducted a shape classification (elongated versus stubby, Fig. 3A) on tool handles and heads in the predefined ROI (Fig. 1A). As shown in Fig. 3C, the shape decoding was successful within handles (decoding between stubby handle vs. elongated handle: average accuracy = 62.25%, $t_{(24)} = 4.50$, one-tailed $P < 0.001$) but not within heads (decoding between stubby head vs. elongated head: average accuracy = 53.50%, $t_{(24)} = 1.18$, one-tailed $P = 0.25$) (all Bonferroni corrected), and the difference between the shape decoding accuracies was statistically significant ($t_{(24)} = 2.29$, two-tailed $P < 0.05$). To test whether this "handle advantage" was driven by greater shape signals available for handle decoding (i.e., difference between within-shape-type similarity and between-shape-type similarity) than that of heads, we compared the two sets of items on perceptual shape similarity, pixel similarity, and gist similarity. No difference was observed (two-sample *t*-test: perceptual shape similarity, $t_{(22)} = -1.14$, two-tailed $P = 0.27$; pixel similarity, $t_{(22)} = 0.57$, two-tailed $P = 0.58$; gist dissimilarity, $t_{(22)} = -0.04$, two-tailed $P = 0.97$). That is, the LOTC seemed to be more sensitive about the shape of the part that serves as handles for tools (i.e., where to grasp), which was not driven by the amount of shape differences between the handle parts and head parts.

4.2.2. The "grasping-role-in-tool" information decoding results in the LOTC

We conducted two additional ROI-based SVM analyses to examine whether the LOTC encodes the "grasping-role-in-tool" information of a tool part for the handle-shape sensitivity to emerge. First, we tested whether the LOTC activity can decode the role of a tool part (a handle or a head) based on either the activation patterns of the entire tool part stimulus set (tool heads vs. tool handles) or the tool part stimulus set within the two shape groups separately (tool heads vs. tool handles within either elongated parts or stubby parts). The results revealed no significant decoding accuracy for the LOTC compared to chance level ($ts_{(24)} < -0.48$, one-tailed $ps > 0.68$). Another ROI-based SVM analysis tested whether the "role-in-tool" information could be embedded within the LOTC activity patterns to the whole object by testing whether the LOTC could decode whether a whole tool has an elongated handle or a stubby one. The LOTC showed decoding accuracy significantly higher than chance (average accuracy = 57.50%, $t_{(24)} = 2.02$, one-tailed $P < 0.05$). Importantly, elongated-handle tools and stubby-handle tools did not differ significantly on any of the potential confounding variates we tested (two-sample t-tests: perceptual shape similarity, $t_{\text{within–between}\ (26)} = 0.73$, two-tailed $P = 0.47$; pixel similarity, $t_{\text{within–between}\ (26)} = -0.02$, two-tailed $P = 0.98$; gist dissimilarity, $t_{\text{within–between}\ (26)} = 0.06$, two-tailed $P = 0.95$; object familiarity, $t_{\text{elongated-handle-tool vs. stubby-handle-tool}\ (6)} = 0.03$, two-tailed $P = 0.98$). These results suggested that the LOTC represents information about whether a particular tool should be grasped by the elongated part or by the stubby part.

4.2.3. The whole-brain part-shape decoding results

We also performed whole-brain searchlight SVM analyses for the part shapes within tool handles and within tool heads respectively. For both searchlight analyses, the only cluster showing effects that survived multiple-comparison correction was located in the low-level visual cortex. We present results under the uncorrected threshold (one-tailed $P < 0.05$, uncorrected) for illustration of any potential trends of patterns beyond the early visual cortex (Fig. 3D and E). In addition to the LOTC and early visual cortex, the left superior parietal lobule (SPL) (peak MNI coordinate: −27, −60, 60), the left inferior parietal lobule (IPL) (peak MNI coordinate: −60, −30, 42) and the right SPL (peak MNI coordinate: 36, −48, 57) showed trends of tool handle shape information decoding. For the tool head shape information, the early visual cortex (bilateral occipital cortex), bilateral superior and middle and inferior frontal cortex, bilateral superior and inferior temporal cortex, left inferior parietal cortex, right superior parietal cortex, right middle temporal cortex, and right thalamus (see Table 1) showed trends of a decoding ability. Within the union of voxels showing a decoding advantage for either the handle or head shape (Fig. 3D and E), a direct contrast of the effect magnitude of shape-within-handle vs. shape-within-head revealed that shape-within-handle had advantages in a cluster in the right occipital cortex (peak voxel at MNI coordinate: 21, −84, −15) passing the corrected threshold and, at a more liberal threshold (Fig. 3F, paired-sample *t*-test, two-tailed $P < 0.005$), in the left LOTC (peak voxel at MNI coordinate: −57, −66, −12) and left occipital cortex (peak voxel at MNI coordinate: −33, −96, 0). Several clusters located in the bilateral occipital cortex, bilateral inferior frontal cortex, bilateral superior and inferior temporal cortex, left postcentral motor cortex, left paracentral lobule, right superior and middle frontal cortex showed advantages in head shape decoding (see Table 1).

4.2.4. The RSA results of experiment 3

ROI-based RSA of Experiment 3 did not reveal any significant effects. Specifically, when whole tools were presented neither the overall shape nor the handle/head shape RSMs correlated with the neural RSM ($rs < -0.05$, one-tailed $ps > 0.61$, uncorrected). When the tool parts were shown in isolation, neither the handle nor head shape RSMs significantly correlated with the neural RSMs ($rs < 0.17$, one-tailed $ps > 0.19$, uncorrected). The null results in the RSA might be caused by the limited number of items and less sensitivity, comparing to SVM, to detect signals (Lewis-Peacock and Norman, 2013).

Table 1
The whole-brain searchlight SVM results in Experiment 3.

Searchlight type	Area	Peak voxel coordinates (MNI space)			Peak *t* value (df = 24)	No. of voxels
		x	y	z		
Handle shape classification (one-tailed $P < 0.05$, cluster ≥ 10, uncorrected)	Bilateral Occipital Lobe (including bilateral LOTC)	24	−84	−9	30.55	2518
	Left Superior Parietal Lobule	−27	−60	60	3.84	135
	Left Inferior Parietal Lobule	−60	−30	42	2.51	22
	Right Superior Parietal Lobule	36	−48	57	4.34	167
Head shape classification (one-tailed $P < 0.05$, cluster ≥ 10, uncorrected)	Bilateral Occipital Lobe (including bilateral LOTC)	−18	−96	−12	19.75	3364
	Left Inferior Frontal Gyrus/Superior Temporal Gyrus/Parahippocampa Gyrus	−27	12	−15	4.82	419
	Left Precentral Gyrus/Superior Frontal Gyrus	−15	−12	72	3.80	124
	Left Inferior Frontal Gyrus	−54	9	27	3.40	83
	Left Middle Frontal Gyrus	−39	48	24	3.02	49
	Left Inferior Parietal Lobule	−51	−54	51	2.63	13
	Left Inferior Parietal Lobule	−36	−42	54	2.55	22
	Left Putamen	−33	−15	0	2.46	13
	Right Superior Parietal Lobule	27	−45	57	3.71	109
	Right Inferior Temporal Gyrus	54	−3	−39	3.25	103
	Right Precuneus	15	−57	57	3.23	100
	Right Middle Temporal Gyrus/Superior Temporal Gyrus	54	−9	−12	3.20	36
	Right Superior Frontal Gyrus	15	45	48	3.02	41
	Right Middle Frontal Gyrus/Inferior Frontal Gyrus	27	36	−18	3.00	44
	Right Middle Frontal Gyrus	54	33	21	2.78	16
	Right Thalamus	12	−15	9	2.22	19
Comparison between handle shape classification accuracy and head shape classification accuracy (two-tailed $P < 0.005$, cluster ≥ 15, uncorrected)	Left Middle Occipital Gyrus	−33	−96	0	5.52	34
	Left Lateral Occipitotemporal Cortex	−57	−66	−12	5.42	15
	Right Lingual Gyrus	21	−84	−15	9.37	125
	Left Inferior Frontal Gyrus/Superior Temporal Gyrus	−21	12	−18	−5.97	119
	Left Postcentral Gyrus	−51	−9	15	−5.84	43
	Left Precuneus	−3	−60	18	−5.79	79
	Left Lingual Gyrus	−15	−60	0	−5.60	17
	Left Paracentral Lobule	−6	−45	69	−4.98	17
	Left Hippocampus	−24	−9	−24	−4.82	87
	Right Superior Frontal Gyrus	15	45	48	−6.74	32
	Right Precuneus	9	−51	45	−5.60	32
	Right Superior Temporal Gyrus	51	−12	−9	−5.56	23
	Right Inferior Temporal Gyrus	45	−6	−33	−5.43	69
	Right Middle Frontal Gyrus/Inferior Frontal Gyrus	27	36	−15	−4.71	26

5. Discussion

In the current study, we tested the type of information being processed in the tool-preferring LOTC region. It has been challenging because the shape of an object is usually correlated with how human manually grasp and use the objects, and because the levels of object shape processing here are open (e.g., holistically or part-based). Combining representation similarity analysis and commonality analysis allowed for the breakdown of both joint effects and unique effects of multiple variables. On the whole-object level, across two experiments, we found that how the object is grasped (for pickup) was the variable that best explained the variance in LOTC activity patterns, and it was not the subjectively rated whole object shape or manner of manipulation. When specific tools made of two conceived parts were tested (Experiment 3), it was found that the LOTC encoded the shape of the object part that was considered the tool "handle" (replicated in a subset of similar stimuli in Experiment 2) and not the "head", which suggested the mapping onto grasping information based on both the whole object (which part is the handle) and parts (sensitivity to only handle parts).

Consistent with previous studies (Peelen and Caramazza, 2012; Bracci and Op de Beeck, 2016; Bracci et al., 2017; Wang et al., 2018), we observed that the whole-object shape similarity pattern, as measured by subjective ratings, for small manipulable objects correlated with LOTC neural activity pattern in the RSA (Experiment 1). However, the commonality analysis between shape and grasping manner revealed that, it is the unique grasping manner information (grasping for pickup) of the tools, which was not reflected in the subjective judgment of the overall tool shapes, made the primary contribution to the explanation of the variance in the LOTC neural activity pattern. The results were robust across common small manipulable objects (Experiment 1) and strictly defined tools (Experiment 2). This grasping for pickup information had greater explanatory power for the LOTC activation pattern than another type of motoric component, the manner of manipulation, whose effect was fully explained by its correlation with the grasping manner. This was consistent with previous studies that suggested that grasping-related properties (Fabbri et al., 2016; J. Chen et al., 2017), but not manipulation information (Peelen and Caramazza, 2012; Wang et al., 2018), were likely to be represented in the LOTC. What is the nature of the grasping-related properties shown in LOTC during tool perception then? Theoretically there are at least two possibilities. One is that it stores the information about how a tool is to be grasped – the grasping manner itself. The other possibility is that it still computes shape, but how shape is organized is by the kind of "values" it offers for grasping. That is, the shapes that offer similar kind of grasping actions are represented by more similar neural activity patterns. While we have shown that the subjectively-rated overall object shape is not the critical

dimension here, the shape of the handle part was. On this level of unit the shape and grasping manner becomes difficult to be teased apart due to their high correlations. In Experiment 3 where handle-part shape was manipulated against overall- and head-shape, we found that handle-shape was decoded here. In Experiment 2 where handle shape and grasping manner were considered together we found the effects of the common variance between handle part shape and tool grasping manner. That is, the shape unit in terms of its indication for grasping manner is a plausible explanation of LOTC representation. Note that the failure of decoding head part is surprising because when grasping to transport a tool, processing of head and handle shape are less relevant to satisfy the goal. It remains to be seen whether people do tend to grasp by the handle even in the "pickup" or "transport" tasks, and whether the LOTC neural responses were modulated by whether it was instructed to grasp by the handle or head. The current data nonetheless showed that even during perception, the part to grasp during typical functional use (handle) information was more relevant for the LOTC.

There has recently been a line of elegant studies showing the constraint and interactions between ventral and dorsal streams in tool processing (Almeida et al., 2013; Q. Chen et al., 2017; Budisavljevic et al., 2018; Garcea et al., 2019). It has been hypothesized that, the parietal action system reads specific tool identity information from the ventral stream, and in turn, the ventral areas receive the action-related information from dorsal to refine the object internal representation (Gallivan and Culham, 2015; van Polanen and Davare, 2015). Considering our package of results together with these findings, we propose that the LOTC plays an essential role in computing grasping information from shape, at least during object perception. LOTC parses both whole-object and part-shape in terms their values for action, generating effects of where to grasp and how to grasp (handle part organization being significant), which communicates with the dorsal system in a more transparent manner. It has been shown that for faces and bodies, the corresponding preferring regions in the earlier hierarchy—the occipital face area (OFA) and the extrastriate body area (EBA)—showed responses to object parts or the accumulation of object parts (Taylor et al., 2007; Liu et al., 2009). For the LOTC, our results suggest a joint effect. Of course, there might be other visual or nonvisual properties that are captured by LOTC activity - the variance being explained by the tested variables were close to 10% (comparing to other studies, a value of r = around 0.3 across both experiments is considered very high, for instance, Peelen et al., 2014 found the r was around 0.1 with perceived shape was represented in the inferior temporal cortex across different subject groups; Bracci et al., 2017 found the r was around 0.1 with perceived shape and manipulation information were represented in the LOTC-tool in different tasks). Our current results do not allow us to attest what may capture the remaining variance in LOTC, but do suggest that the knowledge about the whole-object identity and manipulation for tools is not likely to be computed here, given the lack of positive evidence for the unique contribution of knowledge about whole-object shape (subjectively rated) and manipulation (see also Wang et al., 2018).

In addition to the LOTC's sensitivity to tool-handle shape processing, whole-brain SVM analysis revealed tool head shape computation advantages in several clusters in the frontal cortex and temporal lobe. The frontal cortex has long been assumed to be involved in understanding action goals (Rizzolatti and Craighero, 2004; Rizzolatti and Sinigaglia, 2010; Rizzolatti et al., 2014), and the clusters located at the anterior part of the ventral temporal cortex, including the anterior parahippocampal gyrus and hippocampus, showed association with tool function knowledge in a previous study (Chen et al., 2015). The action goal of using a tool and the function of a tool are closely related to the shape of tools' head parts, and our results further showed that the understanding of the action goal for tools is based on the preferential parsing of tool head information. The whole-brain SVM analysis also revealed that several clusters in the low-level visual cortex showed preferences for handle or head information (Fig. 3F). The occipital involvement has also been reported in a set of studies on tool processing where subjects viewed tool pictures (Garcea and Mahon, 2014; Garcea et al. 2016, 2018), or movies of typical functional grasps relative to atypical functional grasps (Valyear and Culham, 2010). The occipital cortex also showed stronger functional connectivity with tool areas in the parietal cortex during tool transportation relative to tool use (Garcea and Buxbaum, 2019). Considering that we have controlled for a set of low level visual features known to be related to occipital activities (gist similarity, pixel similarity, pixel intensity) and perceptual shape similarity, these results pose new questions about the relation between the occipital lobe and the (higher-order) tool processing network.

In conclusion, by looking at various levels of shape properties and grasping properties, convergent evidence indicates that shape analyses in the tool-preferring LOTC are primarily driven by how they indicate grasping manner, which is computed from both the whole-object shape (where to grasp) and the shape for parts typically being grasped (handles/grasping manner). These results suggest that how visual objects are parsed in high-level visual cortex is tightly driven by the downstream functional responses humans have with them, and activity in the LOTC is the way in which humans motorically interact with them.

Declaration of competing interest

The authors declare no competing financial interests.

CRediT authorship contribution statement

Wei Wu: Conceptualization, Investigation, Formal analysis, Validation, Writing - original draft, Writing - review & editing, Visualization. **Xiaoying Wang:** Conceptualization, Formal analysis, Validation, Writing - review & editing, Project administration, Funding acquisition. **Tao Wei:** Investigation, Formal analysis, Funding acquisition. **Chenxi He:** Investigation, Formal analysis. **Yanchao Bi:** Conceptualization, Writing - original draft, Writing - review & editing, Project administration, Supervision, Funding acquisition.

Acknowledgment

Funding: This work was supported by the National Natural Science Foundation of China (31671128 to Y.B.; 31700999 to T.W.; 31500882 to X.W.), Changjiang Scholar Professorship Award (T2016031 to YB), the Fundamental Research Funds for the Central Universities (2017EYT35 to Y.B.), the 111 Project (BP0719032 to Y.B.) and the Interdisciplinary Research Funds of Beijing Normal University (to Y.B.).

Appendix A. Supplementary data

Supplementary data related to this article can be found at https://doi.org/10.1016/j.neuropsychologia.2020.107340.

Notes

We thank Shijia Fan and Haojie Wen for assistance with data collection. We thank Professor Alfonso Caramazza, Dr. Teresa Schubert and Dr. Ella Striem-Amit for helpful discussion. We are also grateful to all research participants.

References

Almeida, J., Fintzi, A.R., Mahon, B.Z., 2013. Tool manipulation knowledge is retrieved by way of the ventral visual object processing pathway. Cortex 49, 2334–2344. http://dx.doi.org/10.1016/j.cortex.2013.05.004.

Bi, Y., Wang, X., Caramazza, A., 2016. Object domain and modality in the ventral visual pathway. Trends Cogn. Sci. 20, 282–290. http://dx.doi.org/10.1016/j.tics.2016.02.002.

Bonner, M.F., Epstein, R.A., 2018. Computational mechanisms underlying cortical responses to the affordance properties of visual scenes. PLoS Comput. Biol. 14, e1006111 http://dx.doi.org/10.1371/journal.pcbi.1006111.

Bracci, S., Cavina-Pratesi, C., Connolly, J.D., Ietswaart, M., 2016. Representational content of occipitotemporal and parietal tool areas. Neuropsychologia 84, 81–88. http://dx.doi.org/10.1016/j.neuropsychologia.2015.09.001.
Bracci, S., Cavina-Pratesi, C., Ietswaart, M., Caramazza, A., Peelen, M.V., 2012. Closely overlapping responses to tools and hands in left lateral occipitotemporal cortex. J. Neurophysiol. 107, 1443–1456. http://dx.doi.org/10.1152/jn.00619.2011.
Bracci, S., Daniels, N., Op de Beeck, H.P., 2017. Task context overrules object- and category-related representational content in the human parietal cortex. Cerebr. Cortex 27, 310–321. http://dx.doi.org/10.1093/cercor/bhw419.
Bracci, S., Op de Beeck, H.P., 2016. Dissociations and associations between shape and category representations in the two visual pathways. J. Neurosci. 36, 432–444. http://dx.doi.org/10.1523/JNEUROSCI.2314-15.2016.
Budisavljevic, S., Dell'Acqua, F., Castiello, U., 2018. Cross-talk connections underlying dorsal and ventral stream integration during hand actions. Cortex 103, 224–239. http://dx.doi.org/10.1016/j.cortex.2018.02.016.
Capraro, R.M., Capraro, M.M., 2001. Commonality analysis: understanding variance contributions to overall canonical correlation effects of attitude toward mathematics on geometry achievement. Mult Lin Regression Viewpoints 27, 16–23.
Chang, C.-C., Lin, C.-J., 2011. Libsvm. ACM Trans Intelligent Systems Technol 2, 1–27. http://dx.doi.org/10.1145/1961189.1961199.
Chao, L.L., Haxby, J.V., Martin, A., 1999. Attribute-based neural substrates in temporal cortex for perceiving and knowing about objects. Nat. Neurosci. 2, 913–919.
Chen, J., Snow, J.C., Culham, J.C., Goodale, M.A., 2017a. What role does "elongation" play in "tool-specific" activation and connectivity in the dorsal and ventral visual streams? Cerebr. Cortex 28, 1117–1131.
Chen, Q., Garcea, F.E., Almeida, J., Mahon, B.Z., 2017b. Connectivity-based constraints on category-specificity in the ventral object processing pathway. Neuropsychologia 105, 184–196. http://dx.doi.org/10.1016/j.neuropsychologia.2016.11.014.
Chen, Q., Garcea, F.E., Mahon, B.Z., 2015. The representation of object-directed action and function knowledge in the human brain. Cerebr. Cortex 26, 1609–1618.
Efron, B., Tibshirani, R.J., 1994. An Introduction to the Bootstrap. CRC press, Boca Raton, FL.
Erdogan, G., Chen, Q., Garcea, F.E., Mahon, B.Z., Jacobs, R.A., 2016. Multisensory part-based representations of objects in human lateral occipital cortex. J. Cogn. Neurosci. 28, 869–881. http://dx.doi.org/10.1162/jocn_a_00937.
Fabbri, S., Stubbs, K.M., Cusack, R., Culham, J.C., 2016. Disentangling representations of object and grasp properties in the human brain. J. Neurosci. 36, 7648–7662. http://dx.doi.org/10.1523/JNEUROSCI.0313-16.2016.
Gallivan, J.P., Culham, J.C., 2015. Neural coding within human brain areas involved in actions. Curr. Opin. Neurobiol. 33, 141–149. http://dx.doi.org/10.1016/j.conb.2015.03.012.
Gallivan, J.P., McLean, D.A., Valyear, K.F., Culham, J.C., 2013. Decoding the neural mechanisms of human tool use. Elife 2, e00425.
Garcea, F.E., Almeida, J., Sims, M.H., Nunno, A., Meyers, S.P., Li, Y.M., Walter, K., Pilcher, W.H., Mahon, B.Z., 2019. Domain-specific diaschisis: lesions to parietal action areas modulate neural responses to tools in the ventral stream. Cerebr. Cortex 29, 3168–3181. http://dx.doi.org/10.1093/cercor/bhy183.
Garcea, F.E., Buxbaum, L.J., 2019. Gesturing tool use and tool transport actions modulates inferior parietal functional connectivity with the dorsal and ventral object processing pathways. Hum. Brain Mapp. 40, 2867–2883. http://dx.doi.org/10.1002/hbm.24565.
Garcea, F.E., Chen, Q., Vargas, R., Narayan, D.A., Mahon, B.Z., 2018. Task- and domain-specific modulation of functional connectivity in the ventral and dorsal object-processing pathways. Brain Struct. Funct. 223, 2589–2607. http://dx.doi.org/10.1007/s00429-018-1641-1.
Garcea, F.E., Kristensen, S., Almeida, J., Mahon, B.Z., 2016. Resilience to the contralateral visual field bias as a window into object representations. Cortex 81, 14–23. http://dx.doi.org/10.1016/j.cortex.2016.04.006.
Garcea, F.E., Mahon, B.Z., 2014. Parcellation of left parietal tool representations by functional connectivity. Neuropsychologia 60, 131–143. http://dx.doi.org/10.1016/j.neuropsychologia.2014.05.018.
Gibson, K.R., Gibson, K.R., Ingold, T., 1994. Tools, Language and Cognition in Human Evolution. Cambridge University Press, Cambridge (UK).
Greene, M.R., Baldassano, C., Esteva, A., Beck, D.M., Fei-Fei, L., 2016. Visual scenes are categorized by function. J. Exp. Psychol. Gen. 145, 82.
Guggenmos, M., Thoma, V., Cichy, R.M., Haynes, J.D., Sterzer, P., Richardson-Klavehn, A., 2015. Non-holistic coding of objects in lateral occipital complex with and without attention. Neuroimage 107, 356–363. http://dx.doi.org/10.1016/j.neuroimage.2014.12.013.
Hebart, M.N., Bankson, B.B., Harel, A., Baker, C.I., Cichy, R.M., 2018. The representational dynamics of task and object processing in humans. Elife 7, e32816.
Hsu, C.-W., Chang, C.-C., Lin, C.-J., 2003. A Practical Guide to Support Vector Classification.
Kraha, A., Turner, H., Nimon, K., Zientek, L.R., Henson, R.K., 2012. Tools to support interpreting multiple regression in the face of multicollinearity. Front. Psychol. 3, 44. http://dx.doi.org/10.3389/fpsyg.2012.00044.
Kriegeskorte, N., Mur, M., Bandettini, P., 2008a. Representational similarity analysis - connecting the branches of systems neuroscience. Front. Syst. Neurosci. 2, 4. http://dx.doi.org/10.3389/neuro.06.004.2008.
Kriegeskorte, N., Mur, M., Ruff, D.A., Kiani, R., Bodurka, J., Esteky, H., Tanaka, K., Bandettini, P.A., 2008b. Matching categorical object representations in inferior temporal cortex of man and monkey. Neuron 60, 1126–1141. http://dx.doi.org/10.1016/j.neuron.2008.10.043.
Lancaster, J.L., Tordesillas-Gutiérrez, D., Martinez, M., Salinas, F., Evans, A., Zilles, K., Mazziotta, J.C., Fox, P.T., 2007. Bias between MNI and Talairach coordinates analyzed using the ICBM-152 brain template. Hum. Brain Mapp. 28, 1194–1205. http://dx.doi.org/10.1002/hbm.20345.
Lewis-Peacock, J.A., Norman, K.A., 2013. Multi-voxel pattern analysis of fMRI data. The cognitive neurosciences 911–920.
Lewis, J.W., 2006. Cortical networks related to human use of tools. The Neuroscientist 12, 211–231. http://dx.doi.org/10.1177/1073858406288327.
Liu, J., Harris, A., Kanwisher, N., 2009. Perception of face parts and face configurations: an fMRI study. J. Cogn. Neurosci. 22, 203–211.
Mahon, B.Z., Milleville, S.C., Negri, G.A., Rumiati, R.I., Caramazza, A., Martin, A., 2007. Action-related properties shape object representations in the ventral stream. Neuron 55, 507–520. http://dx.doi.org/10.1016/j.neuron.2007.07.011.
Martin, A., 2007. The representation of object concepts in the brain. Annu. Rev. Psychol. 58, 25–45. http://dx.doi.org/10.1146/annurev.psych.57.102904.190143.
Monaco, S., Chen, Y., Medendorp, W.P., Crawford, J.D., Fiehler, K., Henriques, D.Y., 2014. Functional magnetic resonance imaging adaptation reveals the cortical networks for processing grasp-relevant object properties. Cerebr. Cortex 24, 1540–1554. http://dx.doi.org/10.1093/cercor/bht006.
Nimon, K., Lewis, M., Kane, R., Haynes, R.M., 2008. An R package to compute commonality coefficients in the multiple regression case: an introduction to the package and a practical example. Behav. Res. Methods 40, 457–466. http://dx.doi.org/10.3758/brm.40.2.457.
Nimon, K., Oswald, F.L., 2013. Understanding the results of multiple linear regression. Organ. Res. Methods 16, 650–674. http://dx.doi.org/10.1177/1094428113493929.
Nimon, K., Oswald, F.L., Roberts, J.K., 2013. Yhat: Interpreting Regression Effects. R Package version:2.0-0.
Oliva, A., Torralba, A., 2001. Modeling the shape of the scene: a holistic representation of the spatial envelope. Int. J. Comput. Vis. 42, 145–175.
Pedzahur, E., 1997. Multiple Regression in Behavioral Research: Explanation and Prediction. London (UK): Wadsworth, Thompson Learning.
Peelen, M.V., Caramazza, A., 2012. Conceptual object representations in human anterior temporal cortex. J. Neurosci. 32, 15728–15736. http://dx.doi.org/10.1523/JNEUROSCI.1953-12.2012.
Peelen, M.V., He, C., Han, Z., Caramazza, A., Bi, Y., 2014. Nonvisual and visual object shape representations in occipitotemporal cortex: evidence from congenitally blind and sighted adults. J. Neurosci. 34, 163–170. http://dx.doi.org/10.1523/JNEUROSCI.1114-13.2014.
Perini, F., Caramazza, A., Peelen, M.V., 2014. Left occipitotemporal cortex contributes to the discrimination of tool-associated hand actions: fMRI and TMS evidence. Front. Hum. Neurosci. 8, 591. http://dx.doi.org/10.3389/fnhum.2014.00591.
Rizzolatti, G., Cattaneo, L., Fabbri-Destro, M., Rozzi, S., 2014. Cortical mechanisms underlying the organization of goal-directed actions and mirror neuron-based action understanding. Physiol. Rev. 94, 655–706.
Rizzolatti, G., Craighero, L., 2004. The mirror-neuron system. Annu. Rev. Neurosci. 27, 169–192.
Rizzolatti, G., Sinigaglia, C., 2010. The functional role of the parieto-frontal mirror circuit: interpretations and misinterpretations. Nat. Rev. Neurosci. 11, 264.
Seibold, D.R., McPhee, R.D., 1979. Commonality analysis: a method for decomposing explained variance in multiple regression analyses. Hum. Commun. Res. 5, 355–365.
Taylor, J.C., Wiggett, A.J., Downing, P.E., 2007. Functional MRI analysis of body and body part representations in the extrastriate and fusiform body areas. J. Neurophysiol. 98, 1626–1633. http://dx.doi.org/10.1152/jn.00012.2007.
Tomasello, M., 1999. The human adaptation for culture. Annu. Rev. Anthropol. 28, 509–529.
Valyear, K.F., Culham, J.C., 2010. Observing learned object-specific functional grasps preferentially activates the ventral stream. J. Cogn. Neurosci. 22, 970–984. http://dx.doi.org/10.1162/jocn.2009.21256.
van Polanen, V., Davare, M., 2015. Interactions between dorsal and ventral streams for controlling skilled grasp. Neuropsychologia 79, 186–191. http://dx.doi.org/10.1016/j.neuropsychologia.2015.07.010.
Wang, X., Fang, Y., Cui, Z., Xu, Y., He, Y., Guo, Q., Bi, Y., 2016. Representing object categories by connections: evidence from a mutivariate connectivity pattern classification approach. Hum. Brain Mapp. 37, 3685–3697. http://dx.doi.org/10.1002/hbm.23268.
Wang, X., Zhuang, T., Shen, J., Bi, Y., 2018. Disentangling representations of shape and action components in the tool network. Neuropsychologia 117, 199–210. http://dx.doi.org/10.1016/j.neuropsychologia.2018.05.026.
Wurm, M.F., Caramazza, A., Lingnau, A., 2017. Action categories in lateral occipitotemporal cortex are organized along sociality and transitivity. J. Neurosci. 37, 562–575. http://dx.doi.org/10.1523/JNEUROSCI.1717-16.2016.
Xia, M., Wang, J., He, Y., 2013. BrainNet Viewer: a network visualization tool for human brain connectomics. PLoS One 8, e68910.